Kusumah, Ferdi Perdana; Vuorsalo, Simo; Kyyrä, Jorma

Components selection of a direct three-phase to single-phase AC/AC converter for a contactless electric vehicle charger

Published in:
Proceedings of the 2016 18th European Conference on Power Electronics and Applications, EPE 2016 ECCE Europe

DOI:
10.1109/EPE.2016.7695411

Published: 25/10/2016

Document Version
Peer-reviewed accepted author manuscript, also known as Final accepted manuscript or Post-print

Please cite the original version:
Kusumah, F. P., Vuorsalo, S., & Kyyrä, J. (2016). Components selection of a direct three-phase to single-phase AC/AC converter for a contactless electric vehicle charger. In *Proceedings of the 2016 18th European Conference on Power Electronics and Applications, EPE 2016 ECCE Europe* Article 7695411 (European Conference on Power Electronics and Applications). IEEE. https://doi.org/10.1109/EPE.2016.7695411

Components Selection of a Direct Three-Phase to Single-Phase AC/AC Converter for a Contactless Electric Vehicle Charger

Ferdi Perdana Kusumah, Simo Vuorsalo, and Jorma Kyyrä
Department of Electrical Engineering and Automation
School of Electrical Engineering
AALTO UNIVERSITY
P.O. Box 13000
FI-00076 Aalto, Finland
Email: ferdi.kusumah@aalto.fi
URL: http://eea.aalto.fi/en/

Keywords

≪AC/AC converter≫, ≪Battery charger≫, ≪Contactless power supply≫, ≪Electric vehicle≫, ≪Resonant converter≫, ≪Soft switching≫.

Abstract

This paper explains a procedure on how to select resonant circuit components of a unique direct three-phase to single-phase AC/AC converter for a contactless electric vehicle (EV) charger. The topology has a fewer bi-directional switches than a matrix converter and consists of a resonant circuit to utilize a zero-current switching (ZCS) mechanism. The selection goal was to realize a working prototype that does not violate each electrical component's limitations as well as has a low resonant damping ratio since the switches are driven based on a resonant current. Selection methods were based on graphical analysis of damping factor, resonant frequency, and primary circuit voltage and current characteristics derived from dynamic and steady-state models. Simulation results are then presented to validate the selection procedures.

Introduction

Contactless Power Transfer (CPT) system through an inductive coupling mechanism usually consists of primary and secondary pick-up circuits. The main purpose of its usage is to remove direct wire connections which leads to reliability, mobility, and safety improvements. The system can be used as an EV charger to improve EV's charging experience that can increase EV's popularity [1]−[3]. In an environment where only a three-phase AC source is commonly used, it is beneficial in terms of size and cost to use a matrix converter in the primary side of the circuit due to an absence of rectification stage that involves a bulky and expensive DC capacitor. However, the converter has a lot of switches and is using a hard-switching principle that can increase its cost and reduce its lifetime [4].

In [5], the authors proposed a direct three-phase to single-phase AC/AC converter topology for a contactless charger. The converter has a lesser number of bi-directional switches than the matrix converter and it operates using a resonant circuit. In [6], the authors proposed a different modulation strategy which is based on current oscillation to drive the direct converter. The strategy is based on injection and free-oscillation modes which were previously introduced in [7] and [8]. Since the switching of the converter is based on a primary resonant current zero crossing, the current must have a low damping ratio value. High damping ratio leads to a termination of the resonant behavior and will stop the converter operation. From a practical point of view, each component's voltage and current limitations must also not be exceeded. Therefore, a resonant circuit components selection based on dynamic and steady-state models is needed to fulfill the requirements.

A direct AC/AC converter topology and its basic working principle are described briefly in the next section. Derivations of required converter models are given afterwards. Selection method of a proper value for each resonant circuit component is discussed based on the models. Some graphs and analysis from MATLAB and PLECS are presented to verify the method on ideal converter operation. Finally, conclusion of the paper is given.

Circuit configuration

Converter topology is given in Fig. 1a. The primary circuit side contains three bi-directional switches Sa, Sb and Sc connecting three-phase input to a series resonant circuit consisted of inductor L_{p} and capacitor C_{p}. The switches will be used to inject resonant current during the period of maximum absolute value of the input voltages with respect to the neutral line which can be described by:

$$\mathrm{Max}(v) = \mathrm{Max}(|v_{\mathrm{a}}(\mathrm{t})|, |v_{\mathrm{b}}(\mathrm{t})|, |v_{\mathrm{c}}(\mathrm{t})|). \tag{1}$$

This mode will be called an injection mode. On the other hand, Sd switch pair will be utilized in a free-oscillation mode to keep the current oscillating in the resonant circuit [6].

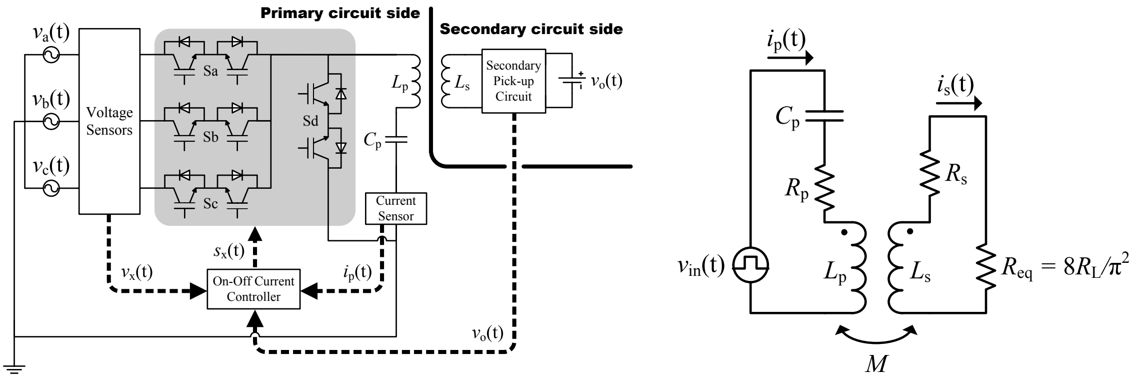

(a) Topology (b) Equivalent circuit

Fig. 1: A Direct three-phase to single-phase AC/AC converter topology and its equivalent circuit.

Both modes (injection and free-oscillation) are controlled by an on-off current controller that receives voltage and current information $v_{\mathrm{x}}(\mathrm{t})$, $v_{\mathrm{o}}(\mathrm{t})$ and $i_{\mathrm{p}}(\mathrm{t})$ to produce $s_{\mathrm{x}}(\mathrm{t})$ gate signals (all are marked by dashed lines). Power is transferred from the primary to the secondary circuit through an inductive coupling mechanism between inductor L_{p} and L_{s}. Some possible current commutations of the primary circuit are given in Fig. 2. Case 1 and 2 correspond to injection modes during $\mathrm{Max}(v) = v_{\mathrm{a}}(\mathrm{t})$ where $v_{\mathrm{a}}(\mathrm{t}) > 0$ and $v_{\mathrm{a}}(\mathrm{t}) < 0$ respectively. The positive sign of the primary current marks its flow to a resonant circuit, while the negative sign indicates its flow to the source. Although the injection modes are demonstrated with only one input phase, the concept is still valid for the other inputs. Free-oscillation mode is described in Case 3 and 4 where the resonant current oscillates in the resonant circuit. Only one of Sd switch pair is connected in each case. Two switches from different pairs with opposite signs ($+$ and $-$) must not be turned-on at the same time to prevent short circuit. Both injection and free-oscillation modes will be used to control the primary current which leads to a controlled secondary current [6].

At a starting phase of the converter, an initial injection (step input) must be applied to one of the input switches (Sa, Sb, or Sc) at a $\mathrm{Max}(v)$ value to start the primary current oscillation. Once the current cross a zero level, a normal operation will be carried out which is illustrated in Fig. 3. It can be seen that during $\mathrm{Max}(v) = v_{\mathrm{b}}(\mathrm{t})$, only Sb$+$ and Sd$-$ switches that are operational. The switching transitions between injection and free-oscillation modes are utilized at zero crossings of primary current $i_{\mathrm{p}}(\mathrm{t})$ to minimize power loss, therefore the switching frequency is equal to the system resonant frequency. A complete explanations of the topology, starting and modulation strategies are given in [6].

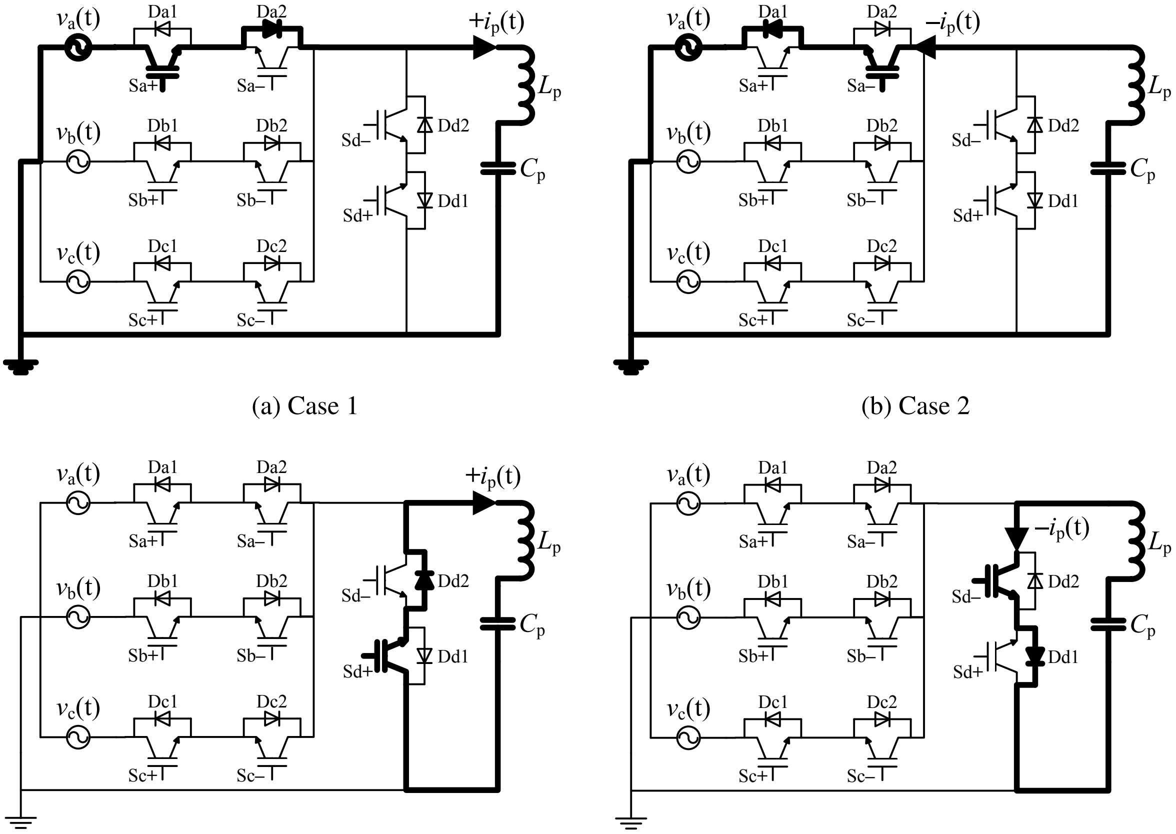

(a) Case 1 (b) Case 2

(c) Case 3 (d) Case 4

Fig. 2: Possible current commutations of the AC/AC converter.

Mathematical model

The resonant circuit components selection is based on dynamic and steady-state models. The models are obtained using an assumption that the converter is running at the Max(v) duration given in (1) with an open-loop control configuration. During this period, only one input phase is used and it is running a successive injection and free-oscillation modes continuously, therefore the primary side can be simplified to a voltage source connected to a series RLC circuit and magnetically coupled to the secondary side. The equivalent circuit is illustrated in Fig. 1b. All passive components are also assumed to be ideal and R_{eq} is used to represent a rectifier and a resistive load R_L based on a fundamental harmonic analysis given in [9]. Capacitor and input voltages are represented by $v_{cp}(t)$ and $v_{in}(t)$ respectively. R_p and R_s represent primary and secondary coil resistances while i_p and i_s indicate primary and secondary circuit currents.

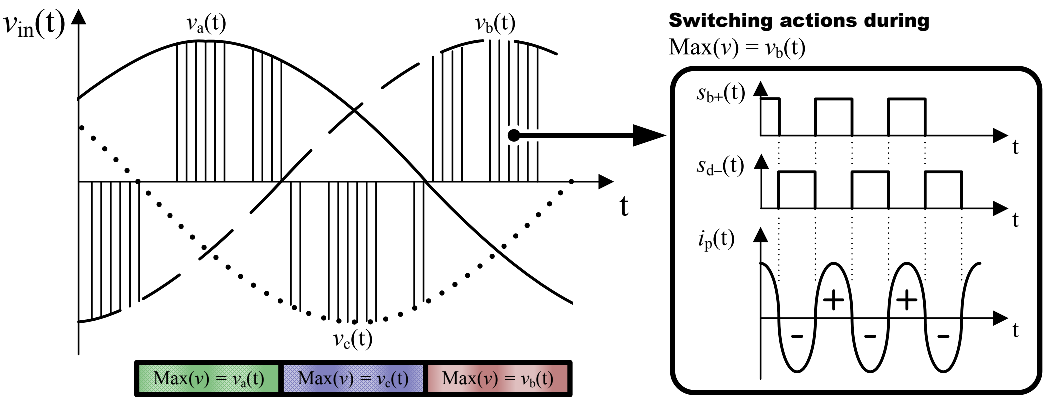

Fig. 3: Switching actions illustration of the AC/AC converter.

Dynamic model representation

A set of ordinary differential equations describing the equivalent circuit in Fig. 1b can be written as follows,

$$
\begin{aligned}
&1.\quad \dot{v}_{\mathrm{cp}}(\mathrm{t}) = \frac{i_{\mathrm{p}}(\mathrm{t})}{C_{\mathrm{p}}},\\
&2.\quad v_{\mathrm{in}}(\mathrm{t}) = v_{\mathrm{cp}}(\mathrm{t}) + i_{\mathrm{p}}(\mathrm{t})R_{\mathrm{p}} + L_{\mathrm{p}}\dot{i}_{\mathrm{p}}(\mathrm{t}) - M\dot{i}_{\mathrm{s}}(\mathrm{t}),\\
&3.\quad 0 = i_{\mathrm{s}}(\mathrm{t})(R_{\mathrm{s}} + R_{\mathrm{eq}}) + L_{\mathrm{s}}\dot{i}_{\mathrm{s}}(\mathrm{t}) - M\dot{i}_{\mathrm{p}}(\mathrm{t}),\\
&4.\quad M = k\sqrt{L_{\mathrm{p}}L_{\mathrm{s}}},
\end{aligned}
\qquad
v_{\mathrm{in}}(\mathrm{t}) = \begin{cases} \mathrm{Max}(v) & \text{if} \quad 0 < \mathrm{t} \leq \frac{T}{2} \\ 0 & \text{if} \quad \frac{T}{2} < \mathrm{t} \leq T, \end{cases} \tag{2}
$$

where M is a mutual inductance and k is a coupling factor that depends on a distance between primary and secondary coils. T is an input voltage switching period which equals to the primary current's oscillation period. The input line voltage frequency is assumed to be much smaller than the switching frequency, as a result, $\mathrm{Max}(v)$ can be approximated by a constant during $0 < \mathrm{t} < \frac{T}{2}$. Therefore, $v_{\mathrm{in}}(\mathrm{t})$ can be considered as an ideal square wave.

To form a state-space for a dynamic analysis, the second and third equations in (2) are inserted to each other to produce,

$$\dot{i}_{\mathrm{p}}(\mathrm{t}) = \frac{1}{L_{\mathrm{p}}L_{\mathrm{s}} - M^2}\Big[L_{\mathrm{s}}v_{\mathrm{in}}(\mathrm{t}) - L_{\mathrm{s}}v_{\mathrm{cp}}(\mathrm{t}) - R_{\mathrm{p}}L_{\mathrm{s}}i_{\mathrm{p}}(\mathrm{t}) - M(R_{\mathrm{s}} + R_{eq})i_{\mathrm{s}}(\mathrm{t})\Big], \tag{3}$$

$$\dot{i}_{\mathrm{s}}(\mathrm{t}) = \frac{1}{L_{\mathrm{p}}L_{\mathrm{s}} - M^2}\Big[Mv_{\mathrm{in}}(\mathrm{t}) - Mv_{\mathrm{cp}}(\mathrm{t}) - MR_{\mathrm{p}}i_{\mathrm{p}}(\mathrm{t}) - L_{\mathrm{p}}(R_{\mathrm{s}} + R_{\mathrm{eq}})i_{\mathrm{s}}(\mathrm{t})\Big]. \tag{4}$$

The state-space is formed using (3), (4) as well as the first equation in (2). The form is given below,

$$
\begin{bmatrix} \dot{v}_{\mathrm{cp}}(\mathrm{t}) \\ \dot{i}_{\mathrm{p}}(\mathrm{t}) \\ \dot{i}_{\mathrm{s}}(\mathrm{t}) \end{bmatrix}
= \underbrace{\begin{bmatrix} 0 & \frac{1}{C_{\mathrm{p}}} & 0 \\ -\frac{L_{\mathrm{s}}}{L_{\mathrm{p}}L_{\mathrm{s}}-M^2} & -\frac{R_{\mathrm{p}}L_{\mathrm{s}}}{L_{\mathrm{p}}L_{\mathrm{s}}-M^2} & -\frac{M(R_{\mathrm{s}}+R_{\mathrm{eq}})}{L_{\mathrm{p}}L_{\mathrm{s}}-M^2} \\ -\frac{M}{L_{\mathrm{p}}L_{\mathrm{s}}-M^2} & -\frac{MR_{\mathrm{p}}}{L_{\mathrm{p}}L_{\mathrm{s}}-M^2} & -\frac{L_{\mathrm{p}}(R_{\mathrm{s}}+R_{\mathrm{eq}})}{L_{\mathrm{p}}L_{\mathrm{s}}-M^2} \end{bmatrix}}_{\mathbf{A}}
\begin{bmatrix} v_{\mathrm{cp}}(\mathrm{t}) \\ i_{\mathrm{p}}(\mathrm{t}) \\ i_{\mathrm{s}}(\mathrm{t}) \end{bmatrix}
+ \underbrace{\begin{bmatrix} 0 \\ \frac{L_{\mathrm{s}}}{L_{\mathrm{p}}L_{\mathrm{s}}-M^2} \\ \frac{M}{L_{\mathrm{p}}L_{\mathrm{s}}-M^2} \end{bmatrix}}_{\mathbf{B}} v_{\mathrm{in}}(\mathrm{t}). \tag{5}
$$

Dynamic model solution

A damping ratio can be calculated from a characteristic equation of (5), but for a completeness purpose, the model will be solved to obtain dynamic responses. By using a Laplace transform approach taken from [10], the state equation can be solved through a matrix integration given in the following form,

$$
\begin{bmatrix} v_{\mathrm{cp}}(\mathrm{t}) \\ i_{\mathrm{p}}(\mathrm{t}) \\ i_{\mathrm{s}}(\mathrm{t}) \end{bmatrix}
= e^{\mathbf{A}\mathrm{t}} \begin{bmatrix} v_{\mathrm{cp}}(0) \\ i_{\mathrm{p}}(0) \\ i_{\mathrm{s}}(0) \end{bmatrix} + \int_0^t e^{\mathbf{A}(\mathrm{t}-\tau)}\mathbf{B}v_{\mathrm{in}}(\tau)d\tau, \qquad e^{\mathbf{A}\mathrm{t}} = \mathcal{L}^{-1}[(\mathrm{s}\mathbf{I} - \mathbf{A})^{-1}]. \tag{6}
$$

Matrices $\mathbf{A}$ and $\mathbf{B}$ come from equation (5). The exponential term can be obtained through an inverse calculation of (s$\mathbf{I}$ - $\mathbf{A}$) prior to applying an inverse Laplace transform as given below,

$$(\mathrm{s}\mathbf{I} - \mathbf{A})^{-1} = \frac{\mathrm{adj}(\mathrm{s}\mathbf{I} - \mathbf{A})}{|\mathrm{s}\mathbf{I} - \mathbf{A}|}, \tag{7}$$

$$|\mathrm{s}\mathbf{I} - \mathbf{A}| = \mathrm{s}^3 + \left[\frac{R_{\mathrm{p}}L_{\mathrm{s}} + L_{\mathrm{p}}(R_{\mathrm{s}} + R_{\mathrm{eq}})}{L_{\mathrm{p}}L_{\mathrm{s}} - M^2}\right]\mathrm{s}^2 + \left[\frac{R_{\mathrm{p}}(R_{\mathrm{s}} + R_{\mathrm{eq}})C_{\mathrm{p}} + L_{\mathrm{s}}}{C_{\mathrm{p}}(L_{\mathrm{p}}L_{\mathrm{s}} - M^2)}\right]\mathrm{s} + \frac{(R_{\mathrm{s}} + R_{\mathrm{eq}})}{C_{\mathrm{p}}(L_{\mathrm{p}}L_{\mathrm{s}} + M^2)}, \tag{8}$$

$$\mathrm{adj}(\mathrm{s}\mathbf{I}-\mathbf{A}) = \begin{bmatrix} \alpha_{1,1}\mathrm{s}^2+\beta_{1,1}\mathrm{s}+\gamma_{1,1} & \alpha_{1,2}\mathrm{s}^2+\beta_{1,2}\mathrm{s}+\gamma_{1,2} & \alpha_{1,3}\mathrm{s}^2+\beta_{1,3}\mathrm{s}+\gamma_{1,3} \\ \alpha_{2,1}\mathrm{s}^2+\beta_{2,1}\mathrm{s}+\gamma_{2,1} & \alpha_{2,2}\mathrm{s}^2+\beta_{2,2}\mathrm{s}+\gamma_{2,2} & \alpha_{2,3}\mathrm{s}^2+\beta_{2,3}\mathrm{s}+\gamma_{2,3} \\ \alpha_{3,1}\mathrm{s}^2+\beta_{3,1}\mathrm{s}+\gamma_{3,1} & \alpha_{3,2}\mathrm{s}^2+\beta_{3,2}\mathrm{s}+\gamma_{3,2} & \alpha_{3,3}\mathrm{s}^2+\beta_{3,3}\mathrm{s}+\gamma_{3,3}, \end{bmatrix}, \quad \alpha_{1,1}=1, \quad \beta_{1,1}=\frac{R_\mathrm{p}L_\mathrm{s}+L_\mathrm{p}(R_\mathrm{s}+R_\mathrm{eq})}{L_\mathrm{p}L_\mathrm{s}-M^2},$$

$$\gamma_{1,1}=\frac{R_\mathrm{p}(R_\mathrm{s}+R_\mathrm{eq})}{L_\mathrm{p}L_\mathrm{s}-M^2}, \quad \alpha_{1,2}=0, \quad \beta_{1,2}=\frac{1}{C_\mathrm{p}}, \quad \gamma_{1,2}=\frac{1}{C_\mathrm{p}}\left[\frac{L_\mathrm{p}(R_\mathrm{s}+R_\mathrm{eq})}{L_\mathrm{p}L_\mathrm{s}-M^2}\right], \quad \alpha_{1,3}=0, \quad \beta_{1,3}=0,$$

$$\gamma_{1,3}=-\frac{1}{C_\mathrm{p}}\left[\frac{M(R_\mathrm{s}+R_\mathrm{eq})}{L_\mathrm{p}L_\mathrm{s}-M^2}\right], \quad \alpha_{2,1}=0, \quad \beta_{2,1}=-\frac{L_\mathrm{s}}{L_\mathrm{p}L_\mathrm{s}-M^2}, \quad \gamma_{2,1}=-\frac{R_\mathrm{s}+R_\mathrm{eq}}{L_\mathrm{p}L_\mathrm{s}-M^2}, \quad \alpha_{2,2}=1,$$

$$\beta_{2,2}=\frac{L_\mathrm{p}(R_\mathrm{s}+R_\mathrm{eq})}{L_\mathrm{p}L_\mathrm{s}-M^2}, \quad \gamma_{2,2}=0, \quad \alpha_{2,3}=0, \quad \beta_{2,3}=-\frac{M(R_\mathrm{s}+R_\mathrm{eq})}{L_\mathrm{p}L_\mathrm{s}-M^2}, \quad \gamma_{2,3}=0, \quad \alpha_{3,1}=0,$$

$$\beta_{3,1}=-\frac{M}{L_\mathrm{p}L_\mathrm{s}-M^2}, \quad \gamma_{3,1}=0, \quad \alpha_{3,2}=0, \quad \beta_{3,2}=-\frac{R_\mathrm{p}M}{L_\mathrm{p}L_\mathrm{s}-M^2}, \quad \gamma_{3,2}=-\frac{1}{C_\mathrm{p}}\left[\frac{M}{L_\mathrm{p}L_\mathrm{s}-M^2}\right],$$

$$\alpha_{3,3}=1, \quad \beta_{3,3}=\frac{R_\mathrm{p}L_\mathrm{s}}{L_\mathrm{p}L_\mathrm{s}-M^2} \quad \gamma_{3,3}=\frac{1}{C_\mathrm{p}}\left[\frac{L_\mathrm{s}}{L_\mathrm{p}L_\mathrm{s}-M^2}\right] \tag{9}$$

The determinant equation in (8) can be represented in its factored form through an analytical method given in [11] or numerically using a MATLAB software. If each root is assumed to be in a complex form of,

$$s_\mathrm{i} = -b_\mathrm{i} - \mathrm{j}c_\mathrm{i}, \qquad \mathrm{i} = 1,2, \text{ and } 3, \tag{10}$$

where b_i and c_i represents real and imaginary number of i^{th} root, the determinant in (8) can be represented generally by,

$$|\mathrm{s}\mathbf{I}-\mathbf{A}| = (\mathrm{s}-s_1)(\mathrm{s}-s_2)(\mathrm{s}-s_3) = (\mathrm{s}+b_1+\mathrm{j}c_1)(\mathrm{s}+b_2+\mathrm{j}c_2)(\mathrm{s}+b_3+\mathrm{j}c_3). \tag{11}$$

By performing a partial fraction expansion to a combination of equation (7), (8), (9) and (11), then applying inverse Laplace transform, the exponential term in (6) becomes,

$$e^{\mathbf{A}\mathrm{t}} = \begin{bmatrix} \phi_{1,1}(\mathrm{t}) & \phi_{1,2}(\mathrm{t}) & \phi_{1,3}(\mathrm{t}) \\ \phi_{2,1}(\mathrm{t}) & \phi_{2,2}(\mathrm{t}) & \phi_{2,3}(\mathrm{t}) \\ \phi_{3,1}(\mathrm{t}) & \phi_{3,2}(\mathrm{t}) & \phi_{3,3}(\mathrm{t}) \end{bmatrix}, \quad \phi_{\mathrm{m,n}}(\mathrm{t}) = \frac{\alpha_{\mathrm{m,n}}\mathrm{s}_1{}^2+\beta_{\mathrm{m,n}}\mathrm{s}_1+\gamma_{\mathrm{m,n}}}{(\mathrm{s}_1-\mathrm{s}_2)(\mathrm{s}_1-\mathrm{s}_3)}e^{\mathrm{s}_1\mathrm{t}} + \frac{\alpha_{\mathrm{m,n}}\mathrm{s}_2{}^2+\beta_{\mathrm{m,n}}\mathrm{s}_2+\gamma_{\mathrm{m,n}}}{(\mathrm{s}_2-\mathrm{s}_1)(\mathrm{s}_2-\mathrm{s}_3)}e^{\mathrm{s}_2\mathrm{t}} + \frac{\alpha_{\mathrm{m,n}}\mathrm{s}_3{}^2+\beta_{\mathrm{m,n}}\mathrm{s}_3+\gamma_{\mathrm{m,n}}}{(\mathrm{s}_3-\mathrm{s}_1)(\mathrm{s}_3-\mathrm{s}_2)}e^{\mathrm{s}_3\mathrm{t}}, \tag{12}$$

where m and n subscripts mark row and column of the exponential matrix respectively. The dynamic model solution in (6) thus becomes,

$$\begin{bmatrix} v_\mathrm{cp}(\mathrm{t}) \\ i_\mathrm{p}(\mathrm{t}) \\ i_\mathrm{s}(\mathrm{t}) \end{bmatrix} = \begin{bmatrix} \phi_{1,1}(\mathrm{t}) & \phi_{1,2}(\mathrm{t}) & \phi_{1,3}(\mathrm{t}) \\ \phi_{2,1}(\mathrm{t}) & \phi_{2,2}(\mathrm{t}) & \phi_{2,3}(\mathrm{t}) \\ \phi_{3,1}(\mathrm{t}) & \phi_{3,2}(\mathrm{t}) & \phi_{3,3}(\mathrm{t}) \end{bmatrix} \begin{bmatrix} v_\mathrm{cp}(0) \\ i_\mathrm{p}(0) \\ i_\mathrm{s}(0) \end{bmatrix} + \int_0^t \begin{bmatrix} \phi_{1,1}(\mathrm{t}-\tau) & \phi_{1,2}(\mathrm{t}-\tau) & \phi_{1,3}(\mathrm{t}-\tau) \\ \phi_{2,1}(\mathrm{t}-\tau) & \phi_{2,2}(\mathrm{t}-\tau) & \phi_{2,3}(\mathrm{t}-\tau) \\ \phi_{3,1}(\mathrm{t}-\tau) & \phi_{3,2}(\mathrm{t}-\tau) & \phi_{3,3}(\mathrm{t}-\tau) \end{bmatrix} \begin{bmatrix} 0 \\ \frac{L_\mathrm{s}}{L_\mathrm{p}L_\mathrm{s}-M^2} \\ \frac{M}{L_\mathrm{p}L_\mathrm{s}-M^2} \end{bmatrix} v_\mathrm{in}(\tau)d\tau. \tag{13}$$

Damping ratio

The damping ratio is defined as a ratio of an exponential decay frequency to a natural frequency ω_n of a second-order system. It characterizes a damped oscillation behavior of the system. In a third-order case, the ratio can be obtained by separating its first and second-order parts. For the second-order part to have an under-damped characteristic, Birkhoff and Mac Lane discriminant D of a cubic equation (in this case, a characteristic equation based on (8)) which is given in [11] has $D > 0$ value. This leads to a single real root and one pair of complex conjugate roots. $D < 0$ and $D = 0$ corresponds to all real roots. Roots of a general second-order transfer-function given in [12] is in the form of,

$$s_{1,2} = -\zeta\omega_{\mathrm{n}} \pm \omega_{\mathrm{n}}\sqrt{\zeta^2-1}, \tag{14}$$

where ζ is the damping ratio. Therefore, for an under-damped third-order system, the ratio can be calculated as follows,

$$\zeta = \frac{|\mathrm{Re}\{s_{\mathrm{z}}\}|}{|s_{\mathrm{z}}|} = \frac{|-\zeta\omega_{\mathrm{n}}|}{\omega_{\mathrm{n}}}, \tag{15}$$

in this case, s_{z} is one of the roots belong to a second-order part of the characteristic equation of (8) [11] [12].

Circuit characteristics

A steady-state analysis of a circuit in Fig. 1b involves a set of equations given below,

$$\begin{cases} V_{\mathrm{s}} = \frac{\mathbf{i_p}}{\mathrm{j}\omega C_{\mathrm{p}}} + \mathbf{i_p}\mathrm{j}\omega L_{\mathrm{p}} + \mathbf{i_p}R_{\mathrm{p}} - \mathbf{i_s}\mathrm{j}\omega M \\ 0 = \mathbf{i_s}R_{\mathrm{eq}} + \mathbf{i_s}\mathrm{j}\omega L_{\mathrm{s}} + \mathbf{i_s}R_{\mathrm{s}} - \mathbf{i_p}\mathrm{j}\omega M, \end{cases} \tag{16}$$

M is given in (2). The value of V_{s} in open-loop mode depends on the switching frequency and is derived in [6]. A RMS value of V_{s} will be used for steady-state calculations. Both equations in (16) can be combined through an elimination of either $\mathbf{i_s}$ or $\mathbf{i_p}$ to produce current expressions given below,

$$\mathbf{i_p} = \frac{V_{\mathrm{s}}}{R_{\mathrm{p}} + \frac{\omega^2M^2(R_{\mathrm{eq}}+R_{\mathrm{s}})}{\omega^2L_{\mathrm{s}}^2+(R_{\mathrm{eq}}+R_{\mathrm{s}})^2} + \mathrm{j}\left[\omega L_{\mathrm{p}} - \frac{1}{\omega C_{\mathrm{p}}} - \frac{\omega^3M^2L_{\mathrm{s}}}{\omega^2L_{\mathrm{s}}^2+(R_{\mathrm{eq}}+R_{\mathrm{s}})^2}\right]}, \tag{17}$$

$$\mathbf{i_s} = \frac{V_{\mathrm{s}}}{\left[\frac{R_{\mathrm{s}}+R_{\mathrm{eq}}+\mathrm{j}\omega L_{\mathrm{s}}}{\mathrm{j}\omega M}\right]\left[R_{\mathrm{p}} + \frac{1}{\mathrm{j}\omega C_{\mathrm{p}}} + \mathrm{j}\omega L_{\mathrm{p}}\right] - \mathrm{j}\omega M}. \tag{18}$$

During a resonant period, this equality condition applies due to an absence of the imaginary part in (17),

$$\omega_0 L_{\mathrm{p}} - \frac{1}{\omega_0 C_{\mathrm{p}}} = \frac{\omega_0^3M^2L_{\mathrm{s}}}{\omega_0^2L_{\mathrm{s}}^2 + (R_{\mathrm{eq}}+R_{\mathrm{s}})^2}, \tag{19}$$

where ω_0 is a resonant frequency of a coupled system between primary and secondary sides. During this condition, the primary and secondary currents become,

$$\mathbf{i}_{\mathbf{p}(\mathrm{res})} = \frac{V_{\mathrm{s}}}{R_{\mathrm{p}} + \frac{\omega_0^2M^2(R_{\mathrm{eq}}+R_{\mathrm{s}})}{\omega_0^2L_{\mathrm{s}}^2+(R_{\mathrm{eq}}+R_{\mathrm{s}})^2}}, \quad \mathbf{i}_{\mathbf{s}(\mathrm{res})} = \frac{V_{\mathrm{s}}}{\frac{R_{\mathrm{p}}L_{\mathrm{s}}}{M} + \frac{\omega_0^2L_{\mathrm{s}}M(R_{\mathrm{s}}+R_{\mathrm{eq}})}{(R_{\mathrm{s}}+R_{\mathrm{eq}})^2+\omega_0^2L_{\mathrm{s}}^2} + \mathrm{j}\left[\frac{\omega_0^3L_{\mathrm{s}}^2M}{(R_{\mathrm{s}}+R_{\mathrm{eq}})^2+\omega_0^2L_{\mathrm{s}}^2} - \frac{R_{\mathrm{p}}(R_{\mathrm{s}}+R_{\mathrm{eq}})-\omega_0^2M^2}{\omega_0 M}\right]}. \tag{20}$$

Primary capacitor and inductor voltages during resonance are given as follows,

$$\mathbf{V_{Cp}} = \frac{\mathbf{i}_{\mathbf{p}(\mathrm{res})}}{\mathrm{j}\omega_0 C_{\mathrm{p}}}, \qquad \mathbf{V_{Lp}} = \mathrm{j}\omega_0 L_{\mathrm{p}}\mathbf{i}_{\mathbf{p}(\mathrm{res})} - \mathrm{j}\omega_0 M\mathbf{i}_{\mathbf{s}(\mathrm{res})} \tag{21}$$

Components selection

The main goal for the components selection is to build a working prototype by considering each resonant circuit component's limitations and a primary current damping behavior. The selection will only be applied to passive components involved in the converter. Selection method will be based on a graphical analysis of several circuit configurations. It is assumed that maximum primary and secondary coil resistances are 0.3 Ω. The input line voltage amplitude is set to 100 V and a ratio of primary and secondary inductances is fixed to one. The components selection step-by-step is briefly introduced as follows:

1. The highest value of a coupling factor (k) is obtained based on a damping ratio (ζ) graphical analysis.
2. The lowest value of a k is chosen qualitatively according to a maximum primary current limitation.
3. Resonant frequencies relative to both k are plotted. By using the results, L_p/C_p ratio and C_p value are selected by taking into account gate driver frequency limit, component's market availability and inductor physical size.
4. Primary circuit components' voltage graphs are used to make sure that the primary capacitor and inductor voltage limits are not exceeded.

Damping ratio analysis

At a starting phase as well as a normal operation of the converter, a ζ that is very close, equals to or greater than one due to k variations, leads to a sudden stop of the converter. The effect will be shown in Simulation results section. Therefore, the k range needs to be limited. Plots of ζ against a secondary circuit resistive load R_L for different k are shown in Fig. 4.

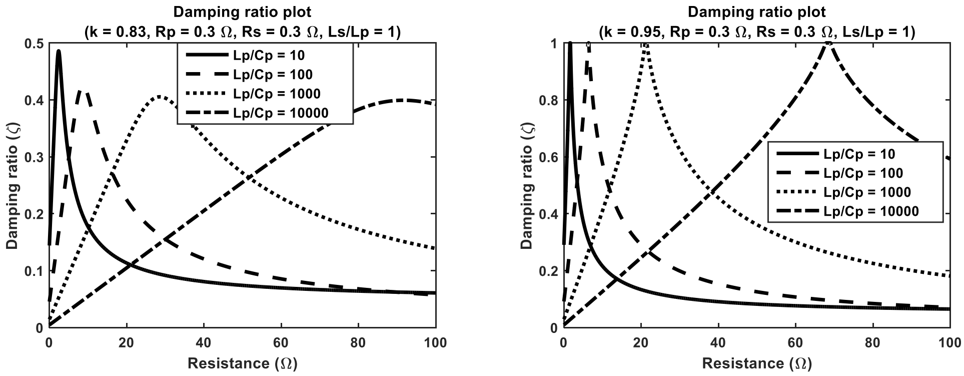

Fig. 4: Damping ratio graphs of the AC/AC converter with different coupling factors. For k = 0.95, the y-axis maximum value is set to one for a clarity purpose.

It can be seen from the right graph of Fig. 4, $k = 0.95$ produces ζ values that reach one for each L_p/C_p ratio. $\zeta > 1$ corresponds to $D < 0$ of the system's characteristic equation. To make sure the $i_p(t)$ sustains oscillation for a certain period of time, a maximum value of $\zeta = 0.5$ is randomly chosen for all circuit configurations. This leads to a selection of k highest value to be $k_{max} = 0.83$ (as shown in the left graph of Fig. 4). A quantitative k_{max} selection based on resonant current settling time and current transducer noise levels will be investigated in future publications.

Primary circuit current analysis

A LEM CASR-6 current transducer was chosen to measure the primary current. Since, it only has a measurement range from -20 A to 20 A, the maximum value of a primary resonant current is set to $I_{max} = 14\ A_{RMS}$. The plots of $\mathbf{i}_{\mathbf{p}(\mathrm{res})}$ with respect to R_L are presented in Fig. 5. From two graphs, at the same R_L value, a lower k corresponds to a higher value of the current amplitude and vice versa. A value of $k_{min} = 0.55$ is then randomly chosen to be the lowest value which makes two plot lines correspond to $L_p/C_p = 1000$ and $L_p/C_p = 10000$ lie under I_{max} for certain load ranges. The ranges are approximately $11.71\ \Omega < R_{eq} < 125.6\ \Omega$ for $k_{min} = 0.55$ and $4.63\ \Omega < R_{eq} < 303\ \Omega$ for $k_{max} = 0.83$. A quantitative selection of k_{min} according to application distance will be studied in the future.

Resonant frequency analysis

The converter input switching frequency is based on a primary current resonance. The value must be chosen based on available gate driver circuits in the market. Power Integrations 2SC0108T was selected due to its affordable price and ease of integration to the main circuit. It has a maximum switching frequency of f_{max} = 50 kHz, therefore the resonant frequency under any condition must be below f_{max}. Plots of the frequency against primary capacitor values based on (19), when $R_L = 0\ \Omega$, are shown in Fig. 6. The lowest R_L corresponds to the highest separation between two coupling factor resonant frequency plots.

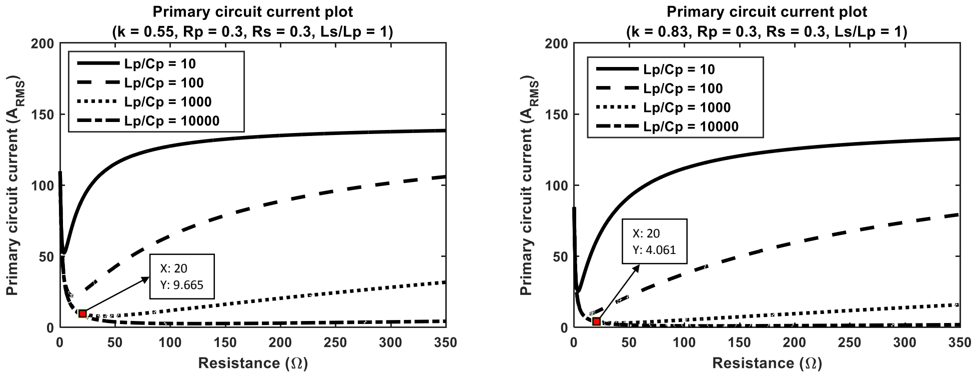

Fig. 5: Primary current graphs under resonance condition.

At the same frequency, the capacitor value is much smaller in $L_p/C_p = 10000$ case compared to $L_p/C_p = 1000$. This leads to a large size of inductor used in both primary and secondary circuits. Thus a ratio of $L_p/C_p = 1000$ is selected. A capacitance of 0.2 μF and an inductance of 200 μH are finally chosen for the resonant circuit. The resonant frequencies of the arrangement with respect to k_{min} and k_{max} are shown by small red squares in Fig. 6.

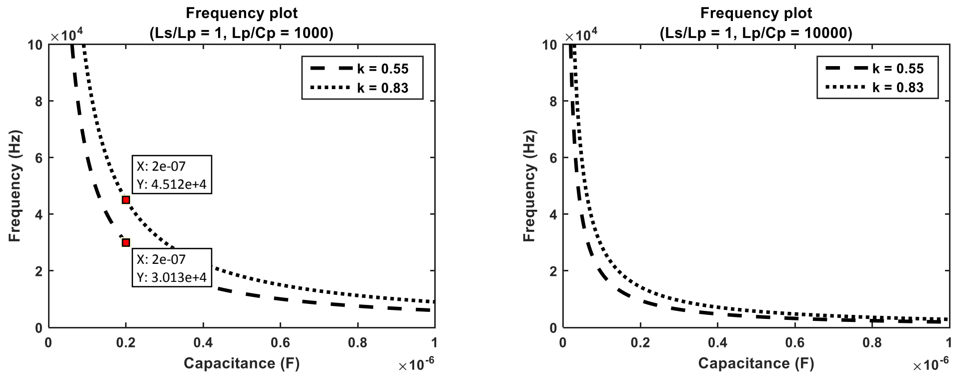

Fig. 6: Resonant frequency graphs of the AC/AC converter when R_p and R_s are 0.3 Ω.

Primary circuit voltages analysis

Capacitor and inductor voltages during resonance under the chosen operational condition must be below their stress limits. This can be investigated through a graphical analysis of the voltages with respect to different R_L values. The graphs are presented in Fig. 7. For a capacitor case, a series connection of ten 2 μF capacitors with each voltage rating of 1000 V can sustain the voltage level at load ranges selected in Primary circuit current analysis. For the inductor, a planar type will be used in the future, therefore the voltage limit depends on coil's number of turns.

Simulation results

High damping ratio

To show the bad effect of a high value of ζ, PLECS software was used. The circuit used in the simulation is based on Fig. 1a, but in this case, the secondary circuit rectifier and load are converted to an equivalent resistance R_{eq}. The converter was set to operate in an open-loop arrangement (successive injection and free-oscillation modes) with $k = 0.908$. The zoomed version of the results are given in Fig. 8. On the left graph, the red ellipse points successive injection switches at an input transition from $\text{Max}(v) = v_a(t)$

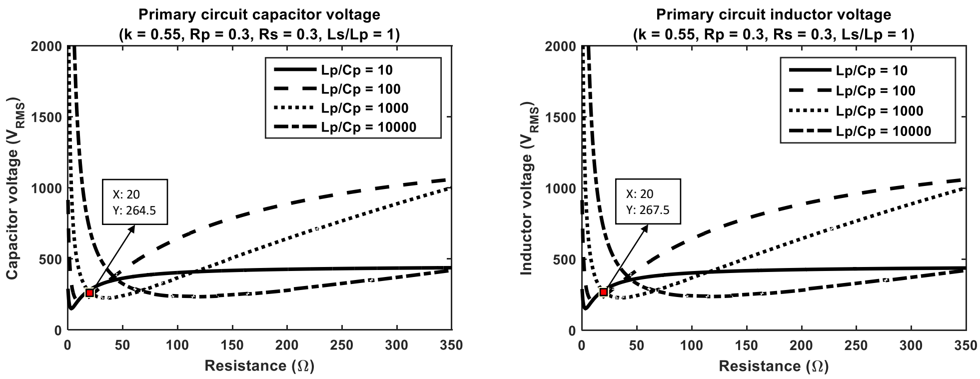

Fig. 7: Primary capacitor and inductor voltages graphs during resonance condition.

to Max(v) = $-v_c$(t). The phenomenon makes the primary current remains oscillating although its shape is skewed. On the right graph, red ellipse indicates successive free-oscillation phases at a transition between Max(v) = $-v_c$(t) to Max(v) = v_b(t) that leads to a sudden halt of a current oscillation. The converter switches are toggling at current zero crossing, therefore in an ideal case, a ζ very close to one will make the current heavily damped and will take a long time to cross the zero level. In a practical case, it may stop the converter operation. It is apparent that a combination of R_L and ζ that produces a critical or over-damped situation must be avoided.

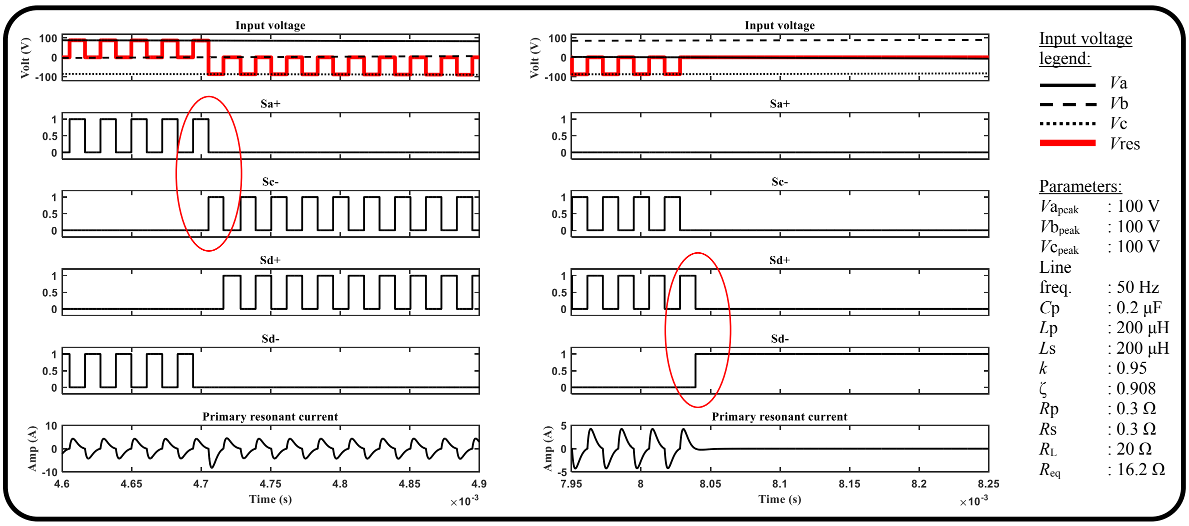

Fig. 8: Simulation results for a high ζ case. V_{res} indicates a voltage over a resonant circuit.

Low damping ratio

PLECS simulation results with configurations from the components selection method is shown in Fig. 9. In this case, the k is changed to 0.55. The data is taken for two periods of input line voltage cycle. Since the switching frequency is much higher than the input line frequency, the switching actions of Sd$-$ and Sd$+$ as well as primary current oscillation cannot be seen clearly. The RMS values of voltages and current from simulation results were taken directly from PLECS scope. A comparison between simulation and analytical calculations is also given in Fig. 9. The analytical results are taken from data points in Fig. 5 and 7 marked by small red squares. The differences are due to an approximation of V_s (steady-state input voltage) mentioned previously in Mathematical model section. From approximately 25 ms onwards, there are current spikes at every transition of input source voltage (one of them is marked by a red ellipse). The spikes are caused by successive injections that produce a current boost at that point as was explained previously in High damping ratio case. The spikes also affect primary capacitor and inductor voltages.

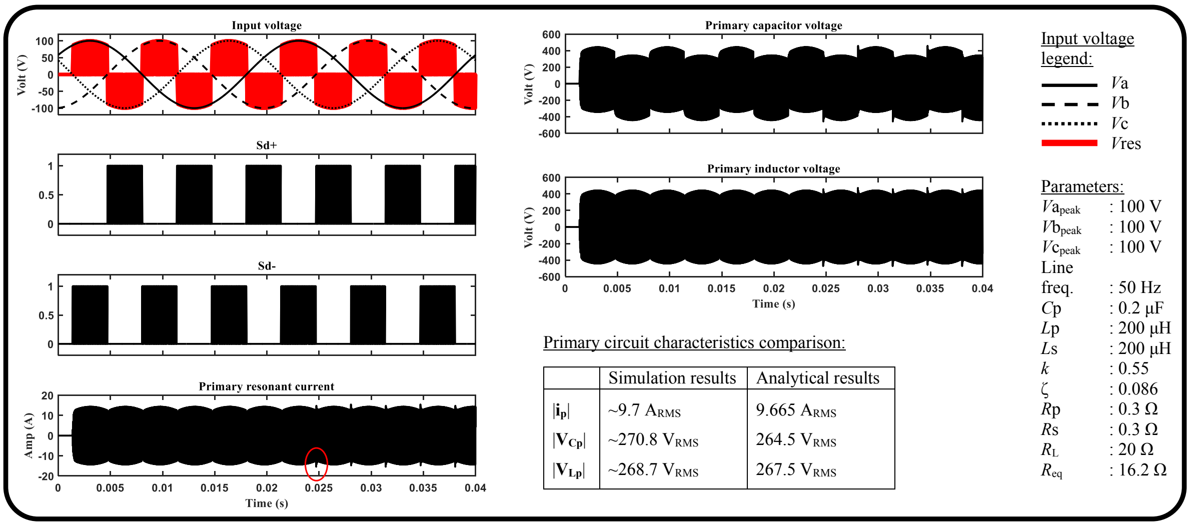

	Simulation results	Analytical results
$\lvert i_p \rvert$	~9.7 A_{RMS}	9.665 A_{RMS}
$\lvert V_{Cp} \rvert$	~270.8 V_{RMS}	264.5 V_{RMS}
$\lvert V_{Lp} \rvert$	~268.7 V_{RMS}	267.5 V_{RMS}

Fig. 9: Simulation results for a low ζ case. V_{res} indicates a voltage over a resonant circuit.

Conclusion

A components selection of a unique direct AC/AC converter for a contactless EV charger has been demonstrated in this paper. The method is based on dynamic and steady-state analyses of its resonant circuit. Since the converter is using a resonance principle, the method will help a designer to avoid a combination of a coupling factor and a load that can stop its operation. The method will also make sure, the converter is working under components' stress limits. Current settling time, transducer's noise level and air-gap distance will be studied in the future and included in the selection method. A working prototype of the converter is currently being built. A practical realization will be reported and analyzed in future publications.

References

[1] M.P. Kazmierkowski and A.J. Moradewicz, "Unplugged but Connected: Review of Contactless Energy Transfer Systems," *IEEE Industrial Electronics Magazine*, vol. 6, pp. 47-55, Dec. 2012.

[2] G.A. Covic and J.T. Boys, "Modern Trends in Inductive Power Transfer for Transportation Applications," *IEEE Journal of Emerging and Selected Topics in Power Electronics*, vol. 1, pp. 28-41, May 2013.

[3] Roman Bosshard *et al.*, "Modeling and η-α-Pareto Optimization of Inductive Power Transfer Coils for Electric Vehicles," *IEEE Journal of Emerging and Selected Topics in Power Electronics*, vol. 3, pp. 50-64, Mar. 2014.

[4] V. Oghafi and A. Radan, "Bidirectional switch commutation for high frequency UPF matrix converter supplying Inductive Power Transfer system," in *Power Electronics, Drive Systems and Technologies Conference*, Tehran, 2014, pp. 422-427.

[5] Nguyen Xuan Bac *et al.*, "A Matrix Converter Based Inductive Power Transfer System," in *International Power & Energy Conference*, Ho Chi Minh City, 2012, pp. 509-514.

[6] F. P. Kusumah *et al.*, "A Direct Three-Phase to Single-Phase AC/AC Converter for Contactless Electric Vehicle Charger," in *European Conference on Power Electronics and Applications*, Geneva, 2015, pp. 1-10.

[7] A. P. Hu and Hao L. Li, "A new high frequency current generation method for inductive power transfer applications," in *IEEE Power Electronics Specialists Conference*, Jeju, 2006, pp. 1-6.

[8] Hao Leo Li *et al.*, "A Direct AC-AC Converter for Inductive Power-Transfer Systems," *IEEE Transactions on Power Electronics*, vol. 27, pp. 661-668, Jun 2011.

[9] R. L. Steigerwald, "A Comparison of Half-Bridge Resonant Converter Topologies," *IEEE Transactions on Power Electronics*, vol. 3, pp. 174-182, Apr 1988.

[10] Katsuhiko Ogata, "Control Systems Analysis in State Space," in *Modern Control Engineering*, 5th ed., Upper Saddle River, NJ: Pearson Education, Inc., 2010, pp. 648-721.

[11] E. W. Weisstein, *CRC Concise Encyclopedia of Mathematics*, Boca Raton, FL: Chapman & Hall/CRC, 2003, pp. 610-613.

[12] N. S. Nise, "Time Response," *Control System Engineering*, 6th ed., Hoboken, NJ: John Wiley & Sons, Inc., 2011, pp. 161-234.